Invited Articles

Role of singularities in hydrodynamics

J. Eggers
School of Mathematics, University of Bristol, University Walk, Bristol BS8 1TW, United Kingdom

(Received 16 June 2018; published 21 November 2018)

Some of the most interesting structures observed in hydrodynamics are best understood as singularities of the equations of fluid mechanics. Examples are drop formation in free-surface flow, shock waves in compressible gas flow, or vortices in potential flow. These examples show that singularities are characteristic for the tendency of the hydrodynamic equations to develop small-scale features spontaneously, starting from smooth initial conditions. As a result, new structures are created, which form the building blocks of more complicated flows. The mathematical structure of singularities is self-similar, and their characteristics are fixed by universal properties. We review recent developments in this field through the lens of one of the great scientific challenges of today: understanding the structure of turbulence.

DOI: 10.1103/PhysRevFluids.3.110503

I. INTRODUCTION

The foundations of modern fluid mechanics undoubtedly were laid by the partial differential equations developed by Euler [1] and Navier [2], to name just the two greatest contributions; see Ref. [3] for a delightful account of history. The great frustration of hundreds of years of subsequent research was that many important observations were not derivable from the fundamental equations, or even seemed in plain contradiction with observation [3]. The most famous of such "paradoxes" is that of D'Alembert [4,5], which observes that a solid body should encounter no resistance in a potential flow, whereas your airline's fuel bill clearly tells you that this is not the case. The paradox can be resolved by allowing the solution to have singularities [6,7], in this case discontinuities of the velocity, which separate a relatively quiet dead zone behind the obstacle from the flow streaming past it. D'Alembert's argument does not apply to this solution, which allows for a greater pressure in front of the body than in the back and thus produces drag.

In contrast to other field theories, the hydrodynamic equations are nonlinear; as a result, few general techniques of solution apply. Nonlinearity implies that an equation produces an ever-changing family of solutions as the amplitude is varied. The most marked such solutions are those which become *singular*, which to us is equivalent to saying that the solution has developed a vanishing length scale. For example, in the case of Kirchhoff's flow past a body, the velocity varies across a shear layer of vanishing thickness, producing an idealized vortex sheet. The nonlinear character of these solutions is clear: two solutions with two different lines of discontinuity cannot be superimposed, since they live on different solution sets. Velocity gradients are infinite across the shear layer: singularities can also be characterized by the fact that either a hydrodynamic variable, or some derivative of it, goes to infinity at a point (or perhaps along a line).

As a result of their vanishing size, singularities are separated from any boundaries, relatively speaking. While the solution of a linear equation is the reflection of whichever boundary condition is imposed, singular solutions are independent of boundary conditions but reflect the structure of the equation: singularities are the fingerprints of a nonlinear equation. This also means that singularities are associated with new structures being born; the difficulty lies in anticipating what these structures might be and finding the corresponding nonlinear solution structure of the equation.

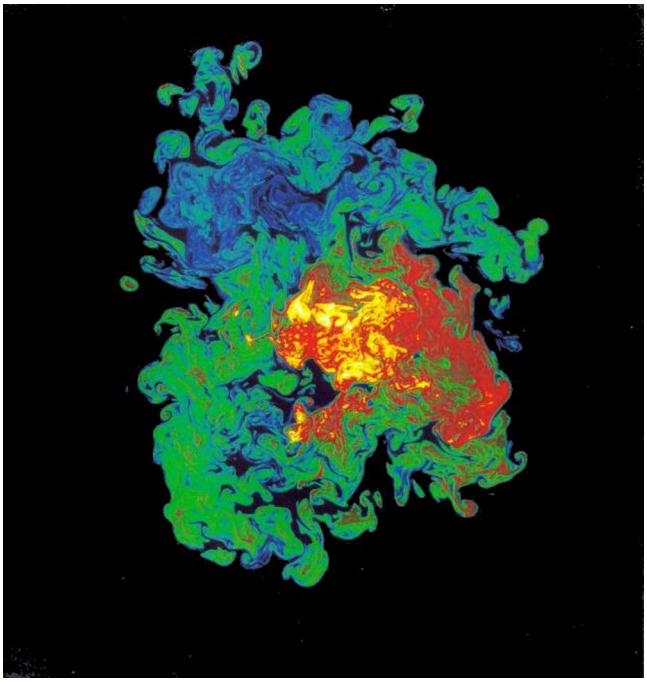

FIG. 1. A turbulent jet injected into another fluid at $\mathrm{Re} = 4.5 \times 10^3$ [12], in a plane normal to the jet axis. The color map codes jet-fluid concentration.

Indeed, some of the most important and influential solutions found in the 19th century are associated with singularities. Apart from the vortex sheets mentioned above, these are the point vortex [8,9], and shock waves of compressible gas dynamics [10,11].

A central research area of 20th-century physics in which the concept of singularities has had a large influence (and to which I was introduced by my thesis advisor, Siegfried Großmann) is that of hydrodynamic turbulence. Richardson [13] introduced the idea of a cascade, which proceeds, by a succession of instabilities, toward smaller and smaller scales. He speculated that this process continuous toward arbitrarily small scales, i.e., singularities form, and certain quantities become nondifferentiable. If the cascade proceeded more or less uniformly in space and energy is conserved along it, this leads to Kolmogorov's famous result that the kinetic energy of velocity fluctuations on scale r scales like $(\epsilon r)^{2/3}$, where ϵ is the rate of energy dissipation [14]. At the Kolmogorov scale $\eta = (\nu^3/\epsilon)^{1/4}$, where ν is the kinematic viscosity, energy is dissipated by viscosity.

However, as illustrated in Fig. 1, in reality turbulence is very nonuniform in space and produces complex spatial structures. The central open problem of turbulence research is to understand this spatial distribution, which has the properties of a multifractal: different regions in space show different scaling properties, which deviate from Kolmogorov's classical result [15]. In the limit of large Reynolds numbers, one might be able to address this problem using the Euler equation alone, where viscosity has been neglected. As has been pointed out by Onsager [16], the Euler equation is able to maintain a stationary turbulent state, in which energy is carried off toward arbitrarily small scales, if only its singularities are sufficiently strong. Such singular solutions could serve as the "coherent structures" which make up the turbulence. Burgers [17] used his own model equation to illustrate this idea, where shock singularities of the velocity profile determine the structure of the turbulence and serve as energy sinks. It is, however, noteworthy that dissipation can potentially produce a singularity which might otherwise be absent [18]. In fact, the first singularity suggested in the turbulence context includes viscosity [19].

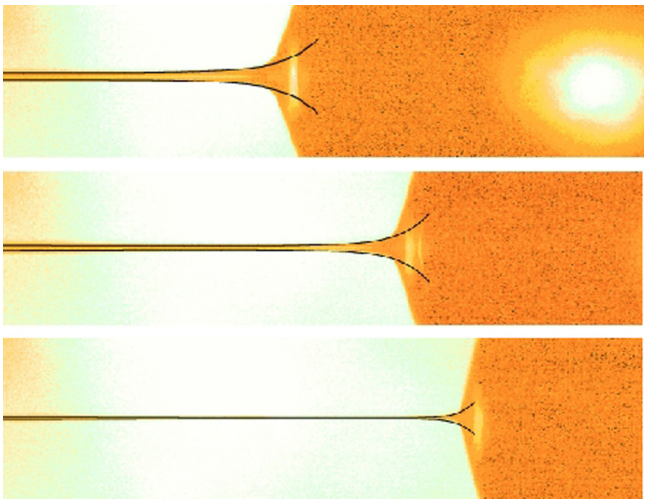

FIG. 2. A sequence of interface profiles of a jet of glycerol of initial radius 0.397 mm (about the width of the image), close to the point of breakup [20] (the center of the drop being formed is seen as a bright spot in the top picture). The experimental images correspond to $t_0 - t = 350\,\mu$s, 298 μs, and 46 μs (from top to bottom). Corresponding analytical solutions based on (1) are superimposed [21]. There is no adjustable parameter in the comparison. The minimum radii for the times shown are $h_{\min} = 153\,\mu$m, 87 μm, and 20 μm, respectively.

I was introduced to a possible connection between singularities and turbulence as a member of Leo Kadanoff's group at the University of Chicago, at a point where the search for singularities of the Euler equation by analytical means had shown little progress, and numerical evidence was ambiguous, a trend that has continued to the present day. Instead, the late Leo Kadanoff suggested that one consider "simpler" singularities, for example, those which occur when a piece of fluid breaks into two [22–24]. Once armed with a sufficient understanding of the mathematical structure of singularities, one might return to the original problem with a greater chance of success.

Since then, the study of such "simple" singularities has taken on a life of its own [25,26] and will presumably continue to do so into the foreseeable future. As an example, in Fig. 2 we show the separation of a drop of liquid from a jet. Let the density be ρ, the kinematic viscosity be ν, and the surface tension, which drives drop formation, γ. Near breakup, the profile becomes long and slender, and the dynamics can be described in terms of its radius $h(z,t)$ (where z is the position along the axis of symmetry) and a mean velocity $v(z,t)$ in the axial direction [27]. Near breakup, where the thread thickness goes to zero, the solution lacks a characteristic length scale, and we expect profiles to assume a scale-invariant form, when measured relative to the point of breakup, assumed to occur at time t_0 and position z_0:

$$h(z,t) = \ell_\nu t' \phi(z'/t'^{1/2}), \quad v(z,t) = (\ell_\nu/t_\nu) t'^{-1/2} \psi(z'/t'^{1/2}). \tag{1}$$

Here $t' = (t_0 - t)/t_\nu$ is the dimensionless time distance to the singularity, and $z' = (z - z_0)/\ell_\nu$ the spatial distance. The length scale $\ell_\nu = \nu^2\rho/\gamma$ and the time scale $t_\nu = \nu^3\rho^2/\gamma^2$ are intrinsic to a given fluid [28] and are thus the proper scales for a phenomenon which is intrinsic to the dynamics and independent of conditions away from the pinch point.

The mathematical content of (1) is that the solution does not change in shape as a function of time, only the axes are rescaled with appropriate powers of t'. As $t' \to 0$, the radius scales as t', while the axial extend of the similarity solution scales like $t'^{1/2}$, which is much larger. This justifies our slenderness assumption and guarantees that the singularity is one-dimensional in character. The shape of the interface is described by the similarity function $\phi(\xi)$, the velocity profile by $\psi(\xi)$, where $\xi = z'/t'^{1/2}$ is the spatial variable in similarity variables.

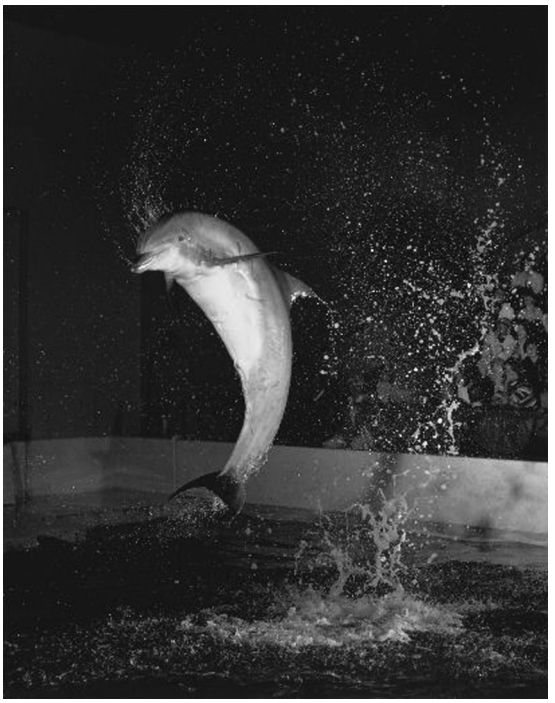

FIG. 3. A dolphin in the New England Aquarium in Boston, MA; Edgerton (1977). ©The Harold E. Edgerton 1992 Trust, courtesy of Palm Press, Inc.

Below we will use the example of a shock wave to explain the workings of a similarity calculation in more detail. In the case of drop breakup, the calculation of the similarity profiles proceeds in two steps [24]: first, the axisymmetric Navier-Stokes equation with a free surface is reduced to a 1+1-dimensional PDE for $h(z,t)$ and $v(z,t)$. Second, the similarity transformation (1) reduces this PDE to a system of ordinary differential equations for ϕ and ψ. These have to be solved numerically and yield the theoretical profiles shown in Fig. 2. A remarkable feature of the calculation is that ϕ and ψ contain no free parameters, so the pinching process can be predicted without reference to the original state of the jet. For example, the minimum of ϕ is $\phi_{\min} = 0.0304\ldots$, leading to the prediction for the minimum thread radius:

$$h_{\min} = 0.0304(\gamma\rho/\nu)(t_0 - t), \tag{2}$$

independent of, e.g., the initial radius of the jet.

To summarize our insights so far, the two salient features of singular solutions are self-similarity and universality [29]. Both are closely related, as they both stem from the fact that singularities evolve on scales widely separated from what might be imposed through boundary conditions or initial conditions. As a result of their universal character, singularities leave their unique fingerprint on even very complex flows, such as that produced by the dolphin in Fig. 3. The most important events in the flow are the formation of new drops, as well as the coalescence of drops, because they lead to a qualitative change in the organization of the flow. Moreover, each singular event repeats itself thousands of times with the same universal features.

This insight leads to a new way of thinking about complex flows: breaking up the flow into a sequence of singularities. Traditionally, the approach to problems in hydrodynamics is dominated by linear stability analysis [30]. In the process, even complex nonlinear phenomena can be understood as a sequence of linear instabilities; see, for example, Ref. [31]. However, without some genuinely nonlinear information about the equations, it is difficult to describe a process across very different

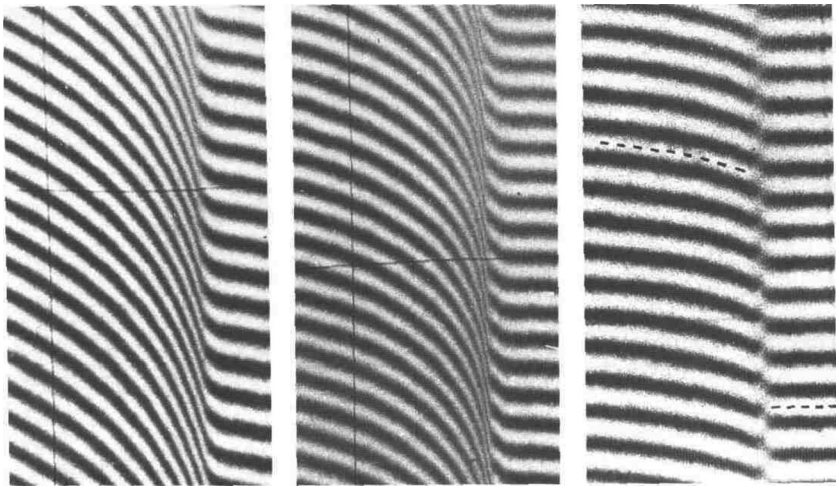

FIG. 4. Fringe pattern showing the steepening of a wave in a gas, leading to the formation of a shock, which is traveling from left to right [32]. The vertical position of a given fringe is proportional to the density at that point. In the last picture a jump of seven fringes occurs.

length scales. In addition, a linear instability always comes with an unknown amplitude, introducing at least one adjustable parameter at each stage. By contrast, nonlinear solutions have the potential to be universal, setting a characteristic amplitude by comparing different (nonlinear) terms in the equation.

In the following, I will try to outline what progress has been made toward Kadanoff's program of studying singularities. This concerns two aspects in particular: the spatial, potentially multifractal complexity found in turbulence, and the organization of the turbulence in two and three dimensions, as opposed to the one-dimensional singularities which have mostly been looked at so far.

II. A SHOCK WAVE: UNDERSTANDING THE STRUCTURE OF A SINGULARITY

We begin with the example of a shock wave propagating in one dimension, as shown in Fig. 4, for which the similarity solution can be calculated analytically. A shock is produced by first creating a compression wave in the tube, which steepens progressively, until a jump is produced at some time t_0. In one dimension, assuming a simple wave [33], compressible gas dynamics can be brought into the form of the kinematic wave equation:

$$u_t + uu_x = 0, \tag{3}$$

where the subscript denotes the derivative. With a dissipative term νu_{xx} on the right-hand side, this is Burgers' equation mentioned earlier.

This inviscid Burgers' equation can easily be solved for any initial condition using the method of characteristics [34], and this exact solution is usually used to describe the shock, without taking notice of its self-similar properties. Instead, here we will describe shock formation using similarity transformations [25,35], which will turn out to be more powerful when we reconsider the problem in higher dimensions.

We take the shock to occur at $t = t_0$ and $x = x_0$; using Galilean invariance, we can make sure that the velocity u vanishes at that point. Then putting $t' = t_0 - t$ and $x' = x = x_0$, in analogy with (1), we make the ansatz

$$u(x,t) = |t'|^{\alpha} U(\xi), \quad \xi = x'/|t'|^{\beta}, \tag{4}$$

where α and β are as yet undetermined scaling exponents. In taking the modulus of t' we anticipate that we also want to look at times $t > t_0$ (where a shock has formed), where t' becomes negative.

Estimating the size of the two terms in (3), we find $u_t \propto |t'|^{\alpha-1}$ and $uu_x \propto |t'|^{2\alpha-\beta}$. For the two terms to balance, we must have $\beta = \alpha + 1$. Inserting the ansatz (4) into (3), we then obtain the similarity equation

$$\pm[-\alpha U + (1+\alpha)\xi U_\xi] + UU_\xi = 0, \tag{5}$$

where the $+$ sign refers to times before shock formation, and the $-$ sign to times after shock formation (the difference in sign comes from the fact that $|t'| = -t'$ after the singularity). We first focus on the time before the singularity, describing the steepening of the wave profile.

Separating variables, for $\alpha \neq 0$ we can write the solution to (5) as

$$\xi = -U - CU^{1+1/\alpha}, \tag{6}$$

where C is a constant of integration. The special case $\alpha = 0$ has the solution $U = -\xi$. However, this yields the unacceptable solution $u = -x'/t'$, which goes to infinity at every point x' as $t' \to 0$, which contradicts the physical expectation that blowup occurs only at a point, whereas the velocity should be finite away from the shock. The exponent α is as yet undetermined, a situation known as self-similarity of the second kind [25,36] [by contrast, in (1) all exponents have been obtained by balancing the different terms in the equation].

Instead, α is determined from the condition that (6) should be regular at the origin; for this to be the case and for (6) to be defined on the whole ξ axis, $1 + 1/\alpha$ must be an odd integer. This leads to

$$\alpha_i = \frac{1}{2i+2}, \quad i = 0, 1, 2 \ldots; \tag{7}$$

the constant C must be positive but is otherwise arbitrary. Thus we have an infinite sequence of possible exponents, and unlike (1) the similarity solution is not completely universal. Instead, C is set by the initial conditions. The next question is which of the sequence of solutions is realized, or perhaps all of them? To answer this, we examine the *stability* of similarity solutions in time, each of which is itself time dependent.

To deal with this difficulty, we introduce the new time variable $\tau = -\ln|t'|$ [37] and search for a generalized similarity solution of the form

$$u(x,t) = t'^{\alpha} U(\xi, \tau); \tag{8}$$

the previous similarity solutions (6) we denote as $\bar{U}(\xi)$ for clarity. Repeating the same steps as before, inserting (8) into (3) yields

$$U_\tau - \alpha U + (1+\alpha)\xi U_\xi + UU_\xi = 0, \tag{9}$$

which we will call the dynamical system [25]. The crucial observation is that the *fixed points* of (9) (for which $U_\tau = 0$) are precisely the solutions of (5) we aim to investigate.

To this end we write

$$U(\xi, \tau) = \bar{U}(\xi) + \delta e^{\nu\tau} P(\xi) \tag{10}$$

and linearize in δ. This yields an eigenvalue equation for perturbations P around the base profile $\bar{U}_i$:

$$(\alpha_i - \nu)P - (1+\alpha_i)\xi P_\xi - P(\bar{U}_i)_\xi - P_\xi \bar{U}_i = 0, \quad i = 0, 1, \ldots, \tag{11}$$

where ν is the eigenvalue. Transforming from the variable ξ to the variable $\bar{U}_i$, we find

$$P\big[(\alpha_i - \nu)\big(1 + (2i+3)\bar{U}_i^{2i+2}\big) + 1\big] = \frac{\partial P}{\partial \bar{U}}\big[\alpha_i \bar{U}_i + (1+\alpha_i)\bar{U}_i^{2i+3}\big], \tag{12}$$

which is once more solved by separation of variables:

$$P = \frac{\bar{U}_i^{3+2i-2\nu(i+1)}}{1+(2i+3)\bar{U}_i^{2i+2}}. \tag{13}$$

The exponent $3+2i-2\nu(i+1)$ must be an integer for (13) to be regular at the origin, so the eigenvalues are

$$\nu_j = \frac{2i+3-j}{2i+2}, \quad j = 0, 1, \ldots. \tag{14}$$

As usual, eigensolutions are alternating between even and odd. However, we are interested only in the *first* instance at which a shock forms. This implies that the second derivative of the profile must vanish at the location of the shock [33], which means that the amplitude of the $j = 2$ perturbation must be exactly zero. Thus for the first similarity solution in the series ($i = 0$), the remaining eigenvalues are $\nu = 3/2, 1, 0, -1/2, \ldots$.

This means there are two positive eigenvalues $3/2$ and 1, which seems to indicate instability, since perturbations in (10) will grow as $\tau \to \infty$, i.e., $t' \to 0$. This is not the case, however; the positive eigenvalues are a result of translational invariance in space and time, and are therefore always present. It is instructive to see why. Namely, if

$$u(x', t') = t'^{\alpha}\bar{U}\left(\frac{x'}{t'^{\beta}}\right)$$

is a similarity solution,

$$u^{(\Delta)}(x', t') = t'^{\alpha}\bar{U}\left(\frac{x'+\Delta}{t'^{\beta}}\right) \equiv t'^{\alpha} f^{(\Delta)}(\xi, \tau) \tag{15}$$

is an equally good solution for any spatial shift Δ. Expanding in Δ we obtain

$$U^{(\Delta)}(\xi, \tau) = \bar{U}(\xi) + \Delta t'^{-\beta}\bar{U}_\xi + O(\Delta^2) \equiv \bar{U} + \Delta e^{\beta\tau}\bar{U}_\xi + O(\Delta^2). \tag{16}$$

But comparing to (10), the term linear in Δ must a solution of (11) with eigenvalue $\nu = \beta$ (which for $i = 0$ is $\beta = \alpha + 1 = 3/2$) and eigenfunction $P(\xi) = \bar{U}_\xi$. In other words, the unstable mode $\bar{U}_\xi$ comes from the fact that a perturbation (of, say, amplitude ϵ) to a similarity solution also leads to a shift $x_0(\epsilon)$. If x_0 is not adjusted accordingly, no blow-up will occur at x_0, which can mean only that one is driven away from the singular solution, which blows up at $x_0(\epsilon)$. Similarly, time translational invariance leads to the eigenvalue $\nu = 1$, the second positive eigenvalue in the series for $i = 0$.

The vanishing eigenvalue comes from the fact that there exists a family of equivalent solutions, parameterized by C. The next largest eigenvalue is $\nu = -1/2$, which corresponds to $i = 0$ being *stable*. Considering the next similarity solution $i = 1$, for which $\alpha_1 = 1/4$, there are two more positive exponents: $\nu = 5/4, 1, 1/2, 1/4$. The first two are accounted for by the above argument, but two more positive values remain, so the solution must be unstable. The same is of course true for all higher order solutions. In conclusion, the only stable solution is $\bar{U}_0$, and the corresponding form of the shock profile is

$$u(x, t) = t'^{1/2}U_b(x'/t'^{3/2}), \tag{17}$$

where U_b is defined implicitly by the third-order curve

$$\xi + U_b + CU_b^3 = 0. \tag{18}$$

This similarity solution is shown on the left of Fig. 5; the subscript b refers to the solution *before* the shock occurs.

Now we proceed to the solution for $t > t_0$, which continues (17). In this case, the similarity equation is (5) with a minus sign, and the solution is

$$\xi - U_a + \bar{C}U_a^{1+1/\alpha} = 0, \tag{19}$$

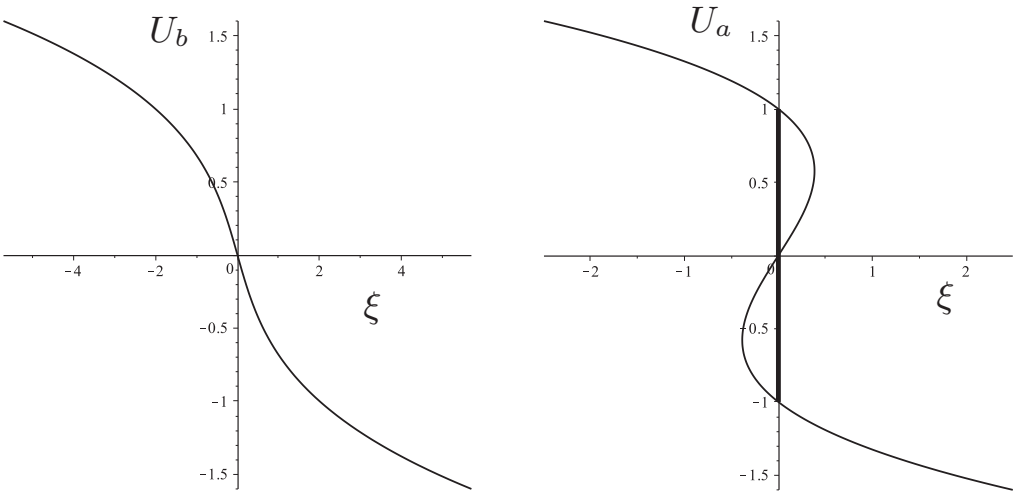

FIG. 5. Similarity solutions before and after the shock. On the left, the solution (18) for $C = 1$; on the right, (21). The curve is nonunique in the center, where the position of the jump (vertical line) is determined by an energy argument.

where $\bar{C}$ is a new constant of integration, and α is *a priori* unknown. The connection with the preshock solution is made by observing that a finite distance Δx away from the singularity, the two solutions must agree as $t' \to 0$: the solutions cannot change instantaneously. This can be formulated as the matching condition

$$\lim_{t'\to 0} u_b(\Delta x, t) = \lim_{t'\to 0} u_a(\Delta x, t), \tag{20}$$

which requires that

$$CU^3 = \bar{C}U^{1+1/\alpha}.$$

However, this can be true only if $\bar{C} = C$ and $\alpha = 1/2$, guaranteeing a unique continuation. The corresponding solution

$$\xi - U_a + CU_a^3 = 0 \tag{21}$$

is plotted in Fig. 5 (right).

There is just one more wrinkle to the argument in the case of shock waves, related to the fact that U_a is not single-valued but overturns. Within this region we have to choose a vertical line, which connects the upper to the lower branch, making the solution single-valued. From (21) it follows that the multivalued region lies in $-2/\sqrt{27C} \leqslant \xi \leqslant 2/\sqrt{27C}$. In real space, this is a region $\Delta x \propto \Delta t^{3/2}$, which has the shape of a cusp; in fact, it can be shown that this is an example of the "cusp singularity" of catastrophe theory [38].

It is well known that on the basis of the equation of motion (3) alone there is no way to choose the horizontal position of the jump. Instead one requires additional conditions to be satisfied across the discontinuity [34], in the case of compressible gas dynamics known as Rankine-Huigoniot conditions [33]. Here, requiring that the flux $u^2/2$ be constant across the discontinuity, it must lie at $\xi = 0$. The height of the jump in (21) is then $2/\sqrt{C}$, which means that in real space the jump in velocity after the singularity grows continuously from zero like $\Delta u = 2\sqrt{|t'|/C}$.

III. COMPLEXITY

One fundamental aspect of turbulent flow is its fractal character, which is usually modeled as a sequence of decays of one structure into several smaller ones. At each step, the characteristic size

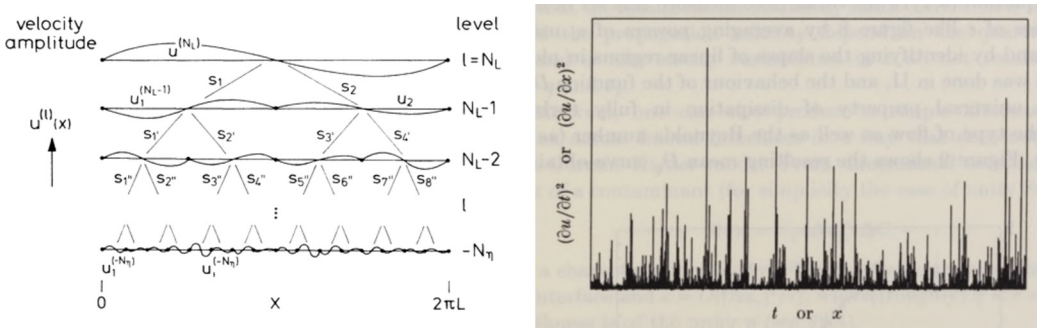

FIG. 6. Left: a fractal cascade is created by breaking up a velocity signal into smaller and smaller pieces [39]. At each stage, the amplitude is multiplied by a (random) factor. On the right, a highly intermittent signal of the local dissipation at high Reynolds numbers [40].

and amplitude of the velocity field decrease, as shown schematically on the left of Fig. 6. If the scale factors s_i are the same at each step and throughout space, the structure has the same scaling properties everywhere; one speaks of a monofractal. If on the other hand scale factors are allowed to fluctuate, the signal becomes extremely rarefied, as indeed is seen in real turbulent signals (cf. Fig. 6, right). Such a structure, which has scaling properties which vary in space, is known as a multifractal [41–43].

By contrast, the smooth self-similar evolution seen during the breakup of a fluid drop in air (see Fig. 2) is not able describe such a structure, even in the simplest case of a monofractal. What is missing is a mechanism by which the same pattern would repeat itself on smaller and smaller scales. However, processes which do produce a pattern have long been seen in other variants of drop breakup, as illustrated in Fig. 7.

Here a fluid filament is suspended in another fluid with a much higher viscosity. As result, as the first breakup event occurs (marked by the square labeled 1), the retraction of the fluid filament that is left behind after breakup is much inhibited, owing to the drag of the outer fluid. Without this inhibition, the fluid filament would have retracted completely into the main drop on the left and a satellite drop in the middle. Instead, as seen most clearly in the blown-up version on the right of Fig. 7, another swell occurs before this can happen. At square 2 another minimum has formed, which leads to breakup in much the same way as at 1. The same process repeats itself at least one more time (square 3), before structures become too small to be recorded.

The repetition or cascade of processes leaves behind a curious structure, which consists of many satellite drops arranged in a fractal pattern, since the drop has become smaller at each stage. Clearly this cannot be described by a fixed point solution of the form (1) or (4), since in that case the same structure evolves smoothly from large to the very smallest scales. It has, however, been recognized for some time [26,45] that such a situation can be realized if the fixed point described by the dynamical system (9) becomes *unstable* and instead develops a periodic orbit of period T in similarity space.

It follows that in that case the evolution is no longer strictly self-similar (that would correspond to the fixed point), but each point along the orbit corresponds to a different spatial profile. However, if one were to catch the evolution at the same phase $\tau_n = \tau_0 + nT$ at each revolution, the same pattern, repeated on smaller and smaller scales, would be observed. From this property the name "discrete self-similarity" derives. Discrete self-similarity would therefore be an ideal candidate for the kinds of repeated structures seen in turbulence. Indeed, it has long been suspected [46,47] that similar structures might describe singularities of the Euler equation; see Ref. [48] for a description of repeated instabilities of vortex filaments into sheets and back into filaments. Numerical evidence of repeated instabilities on smaller and smaller scales has been seen in Ref. [49] in a model for rotating, stratified flow.

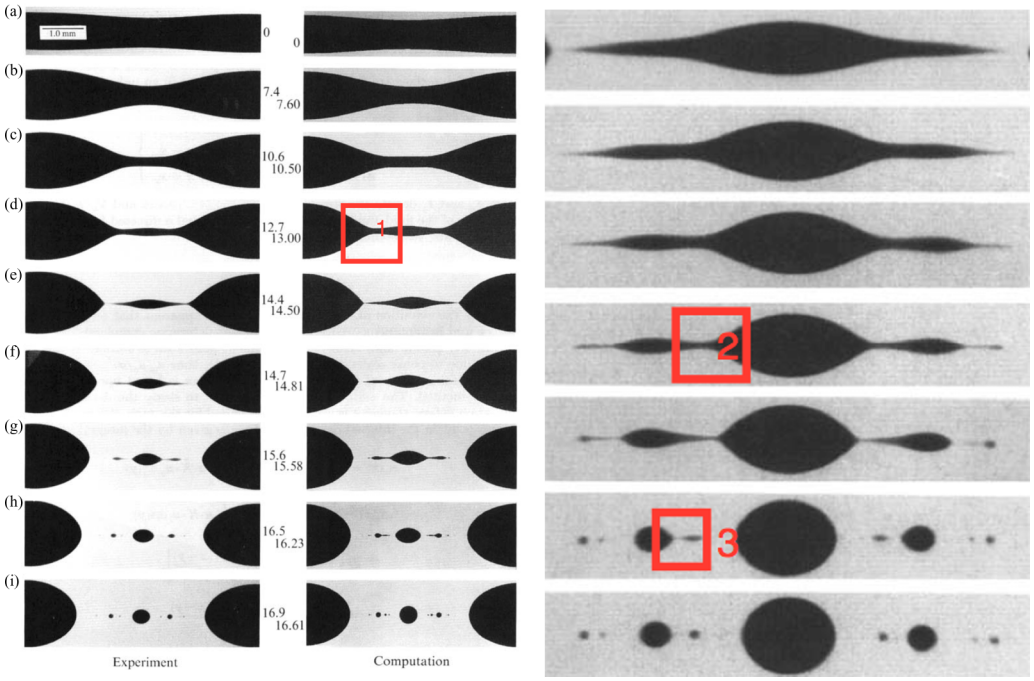

FIG. 7. The breakup of a fluid filament, whose viscosity is smaller by a factor 0.067 relative to the surrounding fluid [44]. On the left, the overall dynamics are compared between theory and experiment; on the right, a blowup of the last stages of the experiment is seen. The same sequence of events repeats itself several times, and three stages of the same event are numbered 1–3.

Unfortunately, most physical examples of discrete self-similarity are quite complicated (a very simple model of such behavior was presented in Ref. [25] as a proof of concept). For example, the two-fluid breakup of Fig. 7 involves multiple breakup events and has never been analyzed on the basis of the underlying equations. However, a new analysis [50] of the equations describing the breakup of a thin film [51,52] has opened the door to an analytical description of complex breakup behavior, using smooth dynamics.

Consider a thin layer of fluid on a solid substrate (we neglect gravity): ordinarily this is a stable situation, as surface tension will only tend to flatten the interface. However, in the case of very thin films (on the order of 10 nm), long-ranged molecular interactions can engender *attractive* power-law interactions between the free interface and the solid substrate, which render the film unstable [53], eventually leading to breakup. If $h(x,t)$ is the film thickness (allowing only for variations in one spatial direction x), the resulting equation of motion is

$$h_t + \left[h^3 \left(h_{xx} - \frac{1}{nh^n} \right)_x \right]_x = 0. \tag{22}$$

The two terms in round brackets correspond to the negative of the pressure in the film, the first coming from surface tension, the second from long-ranged forces. The value of n most often realized on physical grounds is $n = 3$, but here we explore the effect of a "softer" potential for smaller values of n.

Just as in (8) above, we now investigate a possible time dependence in the self-similar behavior of (22):

$$h(x,t) = t'^{\alpha} f(\xi,\tau), \quad \xi = x'/t'^{\beta}, \tag{23}$$

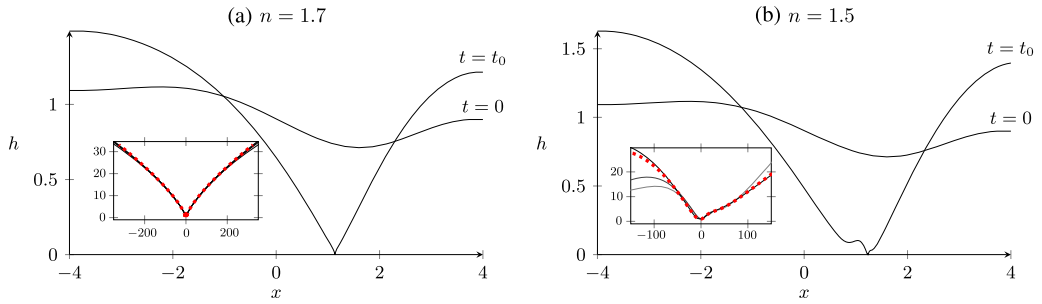

FIG. 8. Two simulations of (22) for the n values indicated [50], from a smooth initial condition up to close to the pinch time $t = t_0$, where $h_{\min} \to 0$. For $n = 1.7$, pinching occurs in a self-similar fashion, corresponding to a fixed point of (24); the self-similar profile $f(\xi)$ is shown in the inset [obtained from rescaling $h(x, t)$ according to (23)] and compared to a solution of the similarity equation (red dots). For $n = 1.5$, pinching is no longer self-similar, but new necks are generated as $t = t_0$ is approached. Collapse (see inset) occurs only if profiles are superimposed in the same phase of the evolution. Red dots are computed from a periodic orbit solution of (24) for which $f_{\min}$ is smallest.

with $\tau = -\ln|t'|$ as before. The exponents are determined from balancing $h_t \sim t'^{\alpha-1}$, $(h^3 h_{xxx})_x \sim t'^{4\alpha-4\beta}$, and $(h^{2-n} h_x)_x \sim t'^{(3-n)\alpha-2\beta}$, from which follows that $\alpha = 1/(2n-1)$, $\beta = (n+1)/(4n-2)$, and the dynamical system is

$$f_\tau = \alpha f - \beta \xi f_\xi - \left[f^3 \left(f_{\xi\xi} - \frac{1}{n f^n} \right)_\xi \right]_\xi . \tag{24}$$

Simulations of the thin film equations (22) are shown in Fig. 8 for two different values of n. For the larger n value, a single self-similar evolution is observed as $h_{\min} \to 0$, described by a τ-independent $f(\xi)$, corresponding to a fixed point solution of (24). To ensure that the similarity solution has a finite limit as $t' \to 0$ outside of the singularity, such a fixed point has to satisfy the condition $\alpha f \sim \beta \xi f_\xi$ as $|\xi| \to \infty$. As for the shock solutions of the kinematic wave equation, for each n there exists an infinity of such similarity solutions, but only the first in the series will concern us here; higher-order solutions are highly unstable. In the inset of Fig. 8(a), numerical solutions $h(x, t)$ are rescaled according to (23) and superimpose perfectly. The red dots come from a solution of the similarity equation [fixed point of (24)] and once more yield the same profile.

However, as seen in Fig. 8(b), for the smaller value of n a completely different picture is observed. A new structure (a little neck) is created as $h \to 0$, and the neck structure repeats itself on even smaller scales. This can be understood by considering the eigenvalue ν of the fixed point as n is lowered. At a critical value $n_c = 1.56\ldots$, the real part of ν goes through zero, to form a pair of complex conjugate eigenvalues $\nu = \pm 0.912i$, in what is known as a Hopf bifurcation [54]. As a result, the fixed point looses stability, to form a time-periodic solution in similarity space. The resulting discrete self-similarity is illustrated in Fig. 9. The system undergoes a periodic evolution in similarity space, during which the profile changes continuously. In order to see a self-similar picture, one has to pick a particular phase and catch the system at exactly the right moment, when this phase returns. In Fig. 8(b) this was done for the profile in the cycle which has the smallest minimum value, as illustrated on the left of Fig. 9. In the inset of Fig. 8(b) one sees the collapse of several profiles, which agree with the corresponding profile found from the dynamical system (24) (red dots).

In the case of a periodic orbit, the same picture repeats itself on smaller and smaller scales, at times $t'_n = e^{-\tau_n} = e^{-\tau_0} e^{-nT}$. This corresponds to a simple fractal, characterized by a single scaling exponent α, with each feature being smaller by a factor of $e^{-\alpha T}$ at each stage. However, one can easily imagine that upon lowering n further, several periodic solutions can appear, which eventually lead to chaotic behavior [26,50], a scenario which had already been anticipated for Euler singularities [47]. Such a possible chaotic behavior is illustrated in Fig. 10 for $n = 1$. Now not only

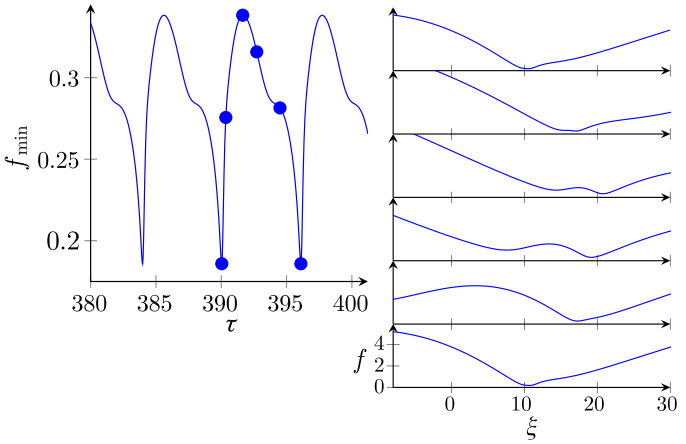

FIG. 9. Periodic solutions of the dynamical system (24) for $n = 1.5$ [50]. On the right, a sequence of similarity profiles $f(\xi, \tau)$, as τ goes through a complete period T. The first and last profiles are identical, as the period is completed. This is illustrated on the left, by plotting the minimum $f_{\min}(\tau)$ of f over ξ as a function of τ. The profiles shown correspond to the dots. The first and last profiles are those for which $f_{\min}$ is smallest.

a single structure but a complex superposition of "satellite drops" of different sizes is seen. It is quite difficult to actually confirm the existence of a chaotic trajectory in such a high-dimensional space, and to confirm its self-similar properties, since the trajectory never comes back to exactly the same point. However, it is tempting to believe that for $n = 1$ a chaotic state is reached, and that the resulting structure exhibits *multifractal* properties—a random superposition of structures with spatially varying scaling properties.

IV. SPATIAL STRUCTURE

We are now coming to the next major question raised by our desire to describe a picture as complex as Fig. 1. A fractal structure can easily be defined in one dimension, but we also want

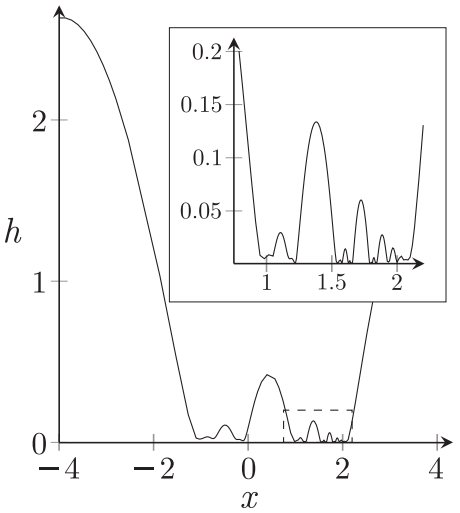

FIG. 10. Complex, and possibly chaotic, dynamics for $n = 1$. The inset shows the ever more complex structure inside the dashed box, near the minimum of the profile.

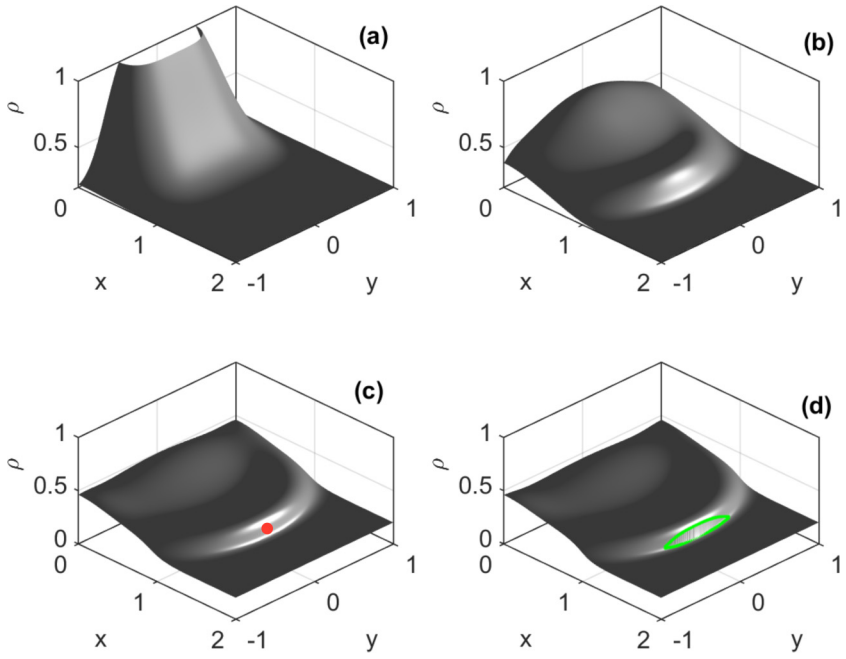

FIG. 11. Time evolution of the density, as described by the compressible Euler equation at $t = 0$ (a), $t = 0.4$ (b), $t = 0.511$ (c), and $t = 0.55$ (d). The initial condition is a localized region of high density in an initially quiescent fluid, with an initial density distribution $\rho(x, y, 0) = 0.2 + e^{-4x^4-4y^2}$. At (c), a shock forms at a point indicated by the red dot, which has spread laterally in (d); the green line indicates the region where the profile has become vertical to within numerical resolution.

to describe patterns in higher dimensions. We address this problem by returning to the problem of shock waves we considered in one dimension in Sec. II. This is illustrated in Fig. 11, which shows the formation of a shock initiated by a peak in density (such a density distribution might be created by an explosion). Generically (unless the distribution is perfectly symmetric), the conditions for a shock (i.e., a discontinuity in the density) will first be met at a point. This is seen in Fig. 11: from (a) (the initial condition) to (b) and (c) the profile gradually steepens. Since the initial profile is steepest along the x axis, the beginning of a shock first occurs on the x axis, as seen in (c). As the height of the jump increases from zero, it spreads in the transversal direction. This region, over which the profile is vertical, is delineated by the green line.

The transversal spread of a shock is illustrated with a physical example in Fig. 12. It shows a plane breaking the sound barrier, producing a shock. As the plane accelerates further, it leaves the initial shock behind, which evolves on its own. The extent of the shock can be traced approximately by the condensation cloud it produces. The width of the cloud in the direction perpendicular to the direction of propagation of the shock is plotted in the figure as a function of the time t from the initiation of the shock. Clearly, the width of the shock scales like a square root of time, which is one of the main features we would like to explain on the basis of the compressible Euler equations, which consists of the balance for mass and linear momentum:

$$\frac{\partial \rho}{\partial t} + \nabla \cdot (\rho \mathbf{v}) = 0, \tag{25}$$

$$\frac{\partial \mathbf{v}}{\partial t} + (\mathbf{v} \cdot \nabla)\mathbf{v} = -\frac{1}{\rho}\nabla p. \tag{26}$$

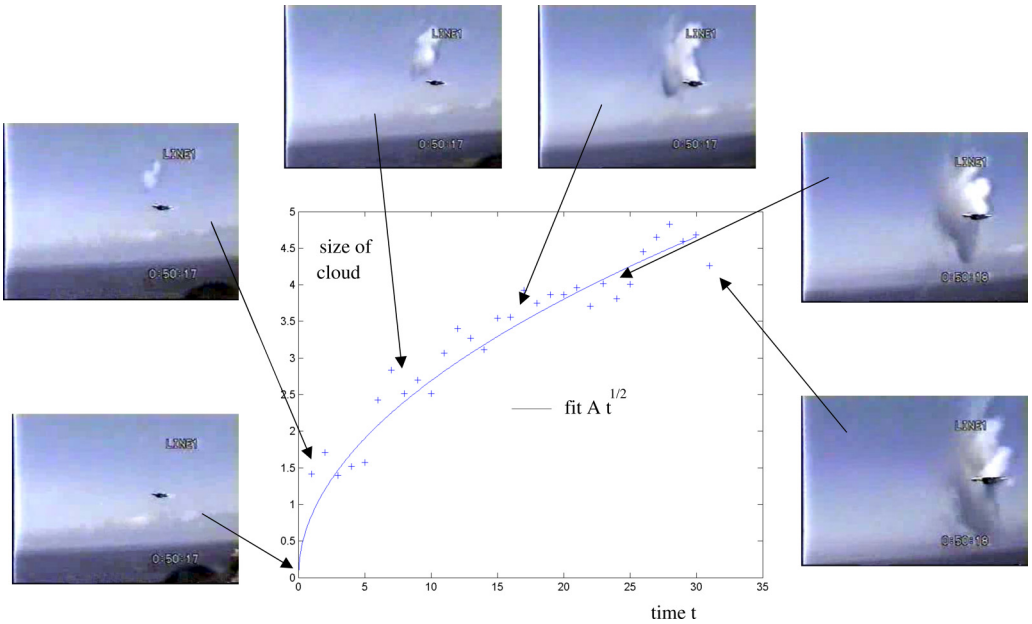

FIG. 12. The spreading of a shock wave behind a supersonic plane, as marked by the condensation cloud produced by the shock. The data are based on measurements from a video [55] with some sample images shown. Image and data analysis by Patrice Legal, used with permission. The width of the cloud scales like $t^{1/2}$, as measured from the initiation of the cloud. Absolute units of space and time are unknown.

In the simplest case of the polytropic ideal gas law, the pressure is just function of density:

$$p = \frac{A}{\gamma}\rho^{\gamma}. \tag{27}$$

In Ref. [56] the higher dimensional shock formation in this system is investigated using similarity solutions. Instead of (4), we are now looking for the two-dimensional similarity structure

$$u(x, y, t) = |t'|^{\alpha} U(\xi, \eta), \quad \xi = x'/|t'|^{\beta_1}, \quad \eta = y'/|t'|^{\beta_2}, \tag{28}$$

for the velocity in the x direction (and analogously for the other fields). We have previously found that $\alpha = 1/2$ and $\beta_1 = 3/2$; we will calculate β_2 based on the idea that the spatial structure in the transversal (y) direction comes mainly from the initial condition. At the center, assumed to be at $y' = 0$, where $y' = y - y_0$, the shock is formed first, at some time t_0. For $y' \neq 0$, on the other hand, the shock forms at some later time $t_c(y') > t_0$. Expanding about $y' = 0$, we must have $t_c(y') - t_0 = ay'^2 + O(y'^3)$, where $a > 0$ [35]. Otherwise the shock would in fact have occurred at some time before t_0. Thus we obtain the scaling $y' \propto t'^{1/2}$, or $\beta_2 = 1/2$.

This means that on the typical scale of the shock region $t'^{3/2}$, conditions vary slowly in the transversal direction, and derivatives in the y direction can be neglected. A more detailed calculation [56] shows that this means we can still use the kinematic wave equation (3), which we have previously studied to study shock formation in one dimension. Since the kinematic wave equation only contains derivatives in the x direction, the spatial structure in the y direction can come only through the initial condition $u_0(x, y)$, as we have anticipated above. Having found the scaling exponents, we can insert

$$u(x, y, t) = |t'|^{1/2} U(\xi, \eta), \quad \xi = x'/|t'|^{3/2}, \quad \eta = y'/|t'|^{1/2}, \tag{29}$$

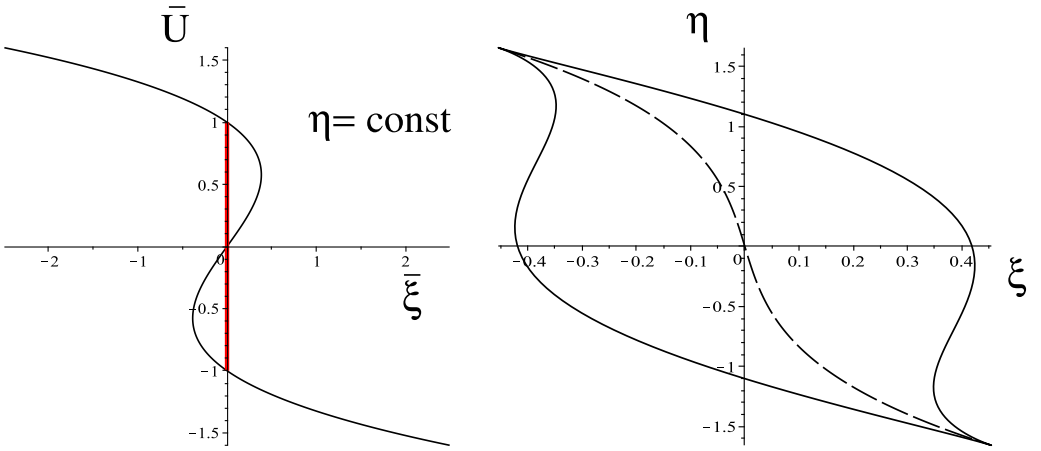

FIG. 13. The structure of the shock in similarity variables. On the left, the equal area construction of Fig. 5, which determines the position of the shock for a fixed value of η. On the right, the lip-shaped region inside which the velocity profile overturns; parameters are $(A_0, A_1, A_2, A_3) = (2, 0.3, 0.5, 0.1)$ and $\gamma = 5/3$. The dashed line marks the position ξ_s of the shock, as found from the construction on the left.

in (3). From the time derivative u_t stems an additional derivative with respect to η, and the previous similarity equation (5) generalizes to

$$U - 3\xi U_\xi - \eta U_\eta = \pm 2 U U_\xi, \tag{30}$$

where the two signs refer to $t < t_0$ and $t > t_0$, respectively.

Now we have to solve the nonlinear partial differential equation (30) in order to understand the spatial structure of the shock. To do that, we once more treat ξ as the dependent variable, and transform to $\xi(U, \eta)$, which yields

$$\xi_U U - 3\xi + \eta \xi_\eta = \pm 2U, \tag{31}$$

which is a linear equation in ξ. One finds by inspection that

$$\xi = \mp U - U^3 F\Big(\frac{\eta}{U}\Big) \tag{32}$$

is a general solution of (31). Thus it seems as if there exist solutions for arbitrary function $F(x)$!

However, one has to once more demand that the solution remains regular at the origin, as we have done in the one-dimensional case. Taking four derivatives on (32), the fourth derivative

$$\frac{\partial^4 \xi}{\partial \eta^4} = -\frac{1}{U} F^{(iv)}\Big(\frac{\eta}{U}\Big)$$

diverges at the origin as $U \to 0$, except if $F^{(iv)}(x)$ vanishes. Thus F must in fact be a third-order polynomial, and the final form of the similarity solution is

$$\xi = \mp \frac{\gamma + 1}{2} U - A_0 U^3 - A_1 U^2 \eta - A_2 U \eta^2 - A_3 \eta^3, \tag{33}$$

for some constants A_0, A_1, A_2, and A_3. In this expression we have restored the exact form valid for the full Euler equation (25)–(27), where γ is the adiabatic exponent.

To describe the significance of this result, we investigate the region within which the profile is multivalued. At constant values of the transversal coordinate η (Fig. 13, left), the profile has the same form as in the one-dimensional case. The multivalued region lies between the points where

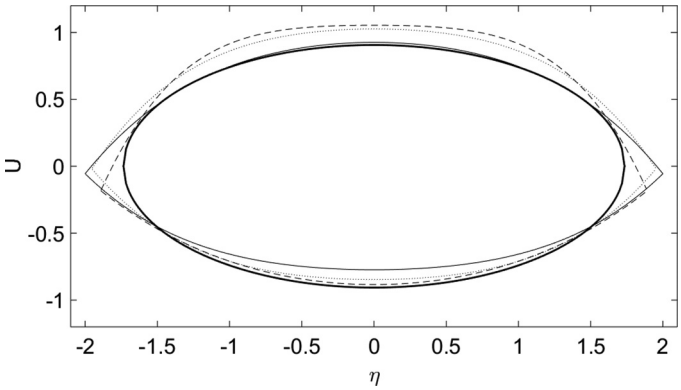

FIG. 14. The rescaled values of the velocity field $U_{1,2}$ at the front and back of the shock, written as a function of the similarity variable η. Numerical results are those of Fig. 11 for $t' = -0.009$ (dashed line), $t' = -0.014$ (dotted line), and $t' = -0.039$ (solid line). The heavy solid line is the theoretical prediction based on (37).

the profile is vertical, i.e., $\partial\xi/\partial U = 0$. Thus for $t > t_0$ we find this region is given by

$$\frac{\gamma+1}{2} = 3A_0U^2 + 2A_1U\eta + A_2\eta^2, \tag{34}$$

which is the lip-shaped region shown in on the right of Fig. 13. To find the position of the shock, we transform the solution (33) to a form equivalent to that of the one-dimensional case. Namely, we introduce shifted variables

$$\bar{\xi} = \xi - \xi_s(\eta), \quad \bar{U} = U - \hat{U}(\eta), \tag{35}$$

so that (33) becomes

$$\bar{\xi} = -A_0\bar{U}[\bar{U}^2 - \Delta^2(\eta)], \tag{36}$$

which is the S-shaped curve shown on the left of Fig. 13. The coefficients $\hat{U}$, ξ_s, and Δ can be found by comparing to (33) [56].

Of particular significance is the height of the jump

$$\Delta = \sqrt{\frac{\gamma+1}{2A_0} + \frac{A_1^2 - 3A_0A_2}{3A_0^2}\eta^2}, \tag{37}$$

which we had previously outlined in Fig. 11(d). The greatest height is at the center of shock, for $\eta = 0$, from where it gradually decreases toward the end. The extent of the shock in the transversal direction is thus determined from $\Delta = 0$, from which we find that the shock region is bound by

$$\eta_\pm = \pm\sqrt{\frac{3A_0(\gamma+1)}{6A_0A_2 - 2A_1^2}}. \tag{38}$$

In real space this means the width of the shock increases like $|t'|^{1/2}$ [with (38) as the prefactor], in agreement with the scaling found in Fig. 12. In Fig. 14 this result is tested in more detail, using the simulation shown in Fig. 11. The ellipse drawn as the solid line is the prediction of theory (37) for the height of the jump as function of the transversal coordinate. The free parameters A_i were determined independently, only using data *before* the singularity, when a shock had not yet formed. Superimposed on it are the velocities $U_{1,2}$ at the front and the back of the shock, as found directly from the simulation, and rescaled according to the similarity solution (29). The

theoretically predicted profiles collapse nicely, and agree with the theoretical prediction without adjustable parameters.

V. OUTLOOK

It is clear that understanding the structure of turbulence remains a daunting task, but it is a great problem to drive us to confront some of the most significant challenges in our field. Singularities are everywhere in hydrodynamics (and in all of continuum mechanics), and we are guaranteed to learn a great deal about how new structures arise as we study them. The self-similar character of singularities greatly simplifies their mathematical structure and makes them amenable to detailed theoretical and quantitative analysis. Making use of scale invariance is perhaps the only general way, across the many subfields of hydrodynamics, to develop an analytical understanding of the nonlinear nature of the underlying equations.

ACKNOWLEDGMENT

Support by the Leverhulme Trust through International Academic Fellowship IAF-2017-010 is gratefully acknowledged.

[1] L. Euler, Principes génereaux du mouvement des fluides, Mem. Acad. Sci. Berlin **11**, 274 (1757).
[2] C. L. Navier, Sur les lois du mouvement des fluides, Mem. Acad. R. Sci. France **6**, 389 (1827).
[3] O. Darrigol, *Worlds of Flow: A History of Hydrodynamics from the Bernoullis to Prandtl* (Oxford University Press, Oxford, 2005).
[4] J. le Rond D'Alembert, Paradoxe proposé aux géometrès sur la résistance des fluides, in *Opuscules mathématiques* (Paris, 1768), Vol. 5, pp. 132–138.
[5] K. Stewartson, D'Alembert's paradox, SIAM Rev. **23**, 308 (1981).
[6] H. Helmholtz, Über diskontinuierliche Flüssigkeitsbewegungen, Monatsber. Berlin Akad., 215 (1868).
[7] G. Kirchhoff, Zur Theorie freier Flüssigkeitsstrahlen, J. Reine Angew. Math. **70**, 289 (1869).
[8] H. Helmholtz, Über Integrale der hydrodynamischen Gleichungen, welche den Wirbelbewegungen entsprechen, J. Reine Angew. Math. **55**, 25 (1858).
[9] S. G. Llewellyn Smith, How do singularities move in potential flow? Physica D **240**, 1644 (2011).
[10] B. Riemann, Über die Fortpflanzung ebener Luftwellen von endlicher Schwingungsweite, Abhandlungen der Gesellschaft der Wissenschaften zu Göttingen, Mathematisch-Physikalische Klasse **8**, 43 (1860).
[11] R. Courant and K. O. Friedrichs, *Supersonic Flow and Shock Waves* (Interscience Publishers, New York, 1948).
[12] P. E. Dimotakis, The mixing transition in turbulent flows, J. Fluid Mech. **409**, 69 (2000).
[13] L. F. Richardson, Atmospheric diffusion shown in a distance-neighbor graph, Proc. R. Soc. London A **110**, 709 (1926).
[14] A. N. Kolmogorov, The local structure of turbulence in incompressible viscous fluid for very large Reynolds' numbers, Dokl. Akad. Nauk SSSR **30**, 301 (1941).
[15] U. Frisch, *Turbulence* (Cambridge University Press, Cambridge, 1995).
[16] G. L. Eyink and K. R. Sreenivasan, Onsager and the theory of hydrodynamic turbulence, Rev. Mod. Phys. **78**, 87 (2006).
[17] J. M. Burgers, A mathematical model illustrating the theory of turbulence, Adv. Appl. Mech. **1**, 171 (1948).
[18] H. K. Moffatt, Euler's disk and its finite-time singularity, Nature (London) **404**, 833 (2000).
[19] J. Leray, Sur le mouvement d'un liquide visqueux emplissant l'espace, Acta Math. **63**, 193 (1934).
[20] T. A. Kowalewski, On the separation of droplets, Fluid Dyn. Res. **17**, 121 (1996).
[21] J. Eggers, Nonlinear dynamics and breakup of free-surface flows, Rev. Mod. Phys. **69**, 865 (1997).

[22] P. Constantin, T. F. Dupont, R. E. Goldstein, L. P. Kadanoff, M. J. Shelley, and S.-M. Zhou, Droplet breakup in a model of the Hele-Shaw cell, Phys. Rev. E **47**, 4169 (1993).
[23] A. L. Bertozzi, M. P. Brenner, T. F. Dupont, and L. P. Kadanoff, Singularities and similarities in interface flows, in *Trends and Perspectives in Applied Mathematics*, Applied Mathematical Sciences Vol. 100, edited by L. Sirovich (Springer, New York, 1994), p. 155.
[24] J. Eggers, Universal Pinching of 3D Axisymmetric Free-Surface Flow, Phys. Rev. Lett. **71**, 3458 (1993).
[25] J. Eggers and M. A. Fontelos, The role of self-similarity in singularities of partial differential equations, Nonlinearity **22**, R1 (2009).
[26] J. Eggers and M. A. Fontelos, *Singularities: Formation, Structure, and Propagation* (Cambridge University Press, Cambridge, 2015).
[27] J. Eggers and T. F. Dupont, Drop formation in a one-dimensional approximation of the Navier-Stokes equation, J. Fluid Mech. **262**, 205 (1994).
[28] D. H. Peregrine, G. Shoker, and A. Symon, The bifurcation of liquid bridges, J. Fluid Mech. **212**, 25 (1990)).
[29] N. Goldenfeld, *Lectures on Phase Transitions and the Renormalization Group* (Addison-Wesley, New York, 1993).
[30] P. G. Drazin and W. H. Reid, *Hydrodynamic Stability* (Cambridge University Press, Cambridge, 1981).
[31] P. Marmottant and E. Villermaux, On spray formation, J. Fluid Mech. **498**, 73 (2004).
[32] W. C. Griffith and W. Bleakney, Shock waves in gases, Am. J. Phys. **22**, 597 (1954).
[33] L. D. Landau and E. M. Lifshitz, *Fluid Mechanics* (Pergamon, Oxford, 1984).
[34] A. Chorin and J. E. Marsden, *A Mathematical Introduction to Fluid Mechanics* (Springer, New York, 1990).
[35] Y. Pomeau, M. Le Berre, P. Guyenne, and S. Grilli, Wave-breaking and generic singularities of nonlinear hyperbolic equations, Nonlinearity **21**, T61 (2008).
[36] G. I. Barenblatt, *Similarity Self-Similarity and Intermediate Asymptotics* (Cambridge University Press, Cambridge, 1996).
[37] Y. Giga and R. V. Kohn, Nondegeneracy of blowup for semilinear heat-equations, Commun. Pure Appl. Math. **42**, 845 (1989).
[38] J. Eggers and N. Suramlishvili, Singularity theory of plane curves and its applications, Eur. J. Mech. B **65**, 107 (2017).
[39] J. Eggers and S. Grossmann, Effect of dissipation fluctuations on anomalous velocity scaling in turbulence, Phys. Rev. A **45**, 2360 (1992).
[40] K. R. Sreenivasan, R. Ramshankar, and C. Meneveau, Mixing, entrainment and fractal dimensions of surfaces in turbulent flows, Proc. Roy. Soc. London A **421**, 79 (1989).
[41] A. N. Kolmogorov, A refinement of previous hypothesis concerning the local structure of turbulence in a viscous incompressible fluid at high Reynold numbers, J. Fluid Mech. **13**, 82 (1962).
[42] B. B. Mandelbrot, Intermittent turbulence in self-similar cascades: Divergence of high moments and dimension of the carrier, J. Fluid Mech. **62**, 331 (1974).
[43] T. C. Halsey, M. H. Jensen, L. P. Kadanoff, I. Procaccia, and B. I. Shraiman, Fractal measures and their singularities: The characterization of strange sets, Phys. Rev. A **33**, 1141 (1986).
[44] M. Tjahjadi, H. A. Stone, and J. M. Ottino, Satellite and subsatellite formation in capillary breakup, J. Fluid Mech. **243**, 297 (1992).
[45] M. W. Choptuik, Universality and Scaling in Gravitational Collapse of a Massless Scalar Field, Phys. Rev. Lett. **70**, 9 (1993).
[46] Y. Pomeau and D. Sciamarella, An unfinished tale of nonlinear PDEs: Do solutions of 3D incompressible Euler equations blow up in finite time? Physica D **205**, 215 (2005).
[47] A. Pumir, B. I. Shraiman, and E. D. Siggia, Vortex morphology and Kelvin's theorem, Phys. Rev. A **45**, R5351 (1992).
[48] M. P. Brenner, S. Hormoz, and A. Pumir, Potential singularity mechanism for the Euler equations, Phys. Rev. Fluids **1**, 084503 (2016).
[49] R. K. Scott and D. G. Dritschel, Numerical Simulation of a Self-Similar Cascade of Filament Instabilities in the Surface Quasigeostrophic System, Phys. Rev. Lett. **112**, 144505 (2014).

[50] M. C. Dallaston, M. A. Fontelos, D. Tseluiko, and S. Kalliadasis, Discrete Self-Similarity in Interfacial Hydrodynamics and the Formation of Iterated Structures, Phys. Rev. Lett. **120**, 034505 (2018).
[51] W. W. Zhang and J. R. Lister, Similarity solutions for Van der Waals rupture of thin film on a solid substrate, Phys. Fluids **11**, 2454 (1999).
[52] T. P. Witelski and A. J. Bernoff, Dynamics of three-dimensional thin film rupture, Physica D **147**, 155 (2000).
[53] D. Bonn, J. Eggers, J. Indekeu, J. Meunier, and E. Rolley, Wetting and spreading, Rev. Mod. Phys. **81**, 739 (2009).
[54] P. G. Drazin, *Nonlinear Systems* (Cambridge University Press, Cambridge, 1992).
[55] https://www.youtube.com/watch?v=gWGLAAYdbbc
[56] J. Eggers, T. Grava, M. A. Herrada, and G. Pitton, Spatial structure of shock formation, J. Fluid Mech. **820**, 208 (2017).